

Article

# Mössbauer Analysis of Deformation–Induced Acceleration of Short-Range Concentration Separation in Fe-Cr Alloys—Effect of the Substitution Impurity: Sb and Au

Valery Shabashov , Kirill Kozlov , Yurii Ustyugov, Andrey Zamatovskii, Timofey Tolmachev  and Evgenii Novikov

Mikheev Institute of Metal Physics, Ural Branch, Russian Academy of Sciences, 620108 Ekaterinburg, Russia; kozlov@imp.uran.ru (K.K.); ustyugov@imp.uran.ru (Y.U.); zamatovsky@imp.uran.ru (A.Z.); tolmachev@imp.uran.ru (T.T.); evg\_nov@mail.ru (E.N.)

\* Correspondence: shabashov@imp.uran.ru

Received: 29 April 2020; Accepted: 28 May 2020; Published: 29 May 2020



**Abstract:** The effect of doping the ferrite alloy Fe-16Cr by the oversized impurities Sb and Au on the mechanism of the short-range ordering induced by “warm” severe plastic deformation was studied using the method of Mössbauer spectroscopy. A comparison between the results obtained and the positron annihilation data on the evolution of the defects of vacancy type stabilized by the impurities Sb and Au was performed. It has been established that the impurities Sb and Au entail a shift of the temperature region of short-range ordering realization in conditions of applying pressure torsion towards greater temperatures by 250 and 100 K, respectively.

**Keywords:** Fe-Cr alloys; severe plastic deformation; substitution impurities; solid solutions; short-range ordering; point defects; Mössbauer spectroscopy

## 1. Introduction

A saturation of the structure of metallic systems upon their severe (mega) plastic deformation with point defects is a feature typical of dissipation of a great amount of mechanical energy in these systems, a consequence of which are the anomalous phase transitions occurring at relatively moderate temperatures, dynamic recrystallization, non-equilibrium and equilibrium atomic diffusion, as well as nanostructurization [1–5]. In a number of iron-based alloys, there has already been shown the twofold effect of severe plastic deformation on the processes of atomic redistribution: on the one hand, disordering stipulated by movement of dislocations and, on the other hand, ordering taking place due to generating moveable vacancy complexes [3,6–8]. In this case, the result of influence depends on the temperature of the influence and is determined by concurrency of the processes of disordering (preferentially at “cold” deformation,  $T \leq T_{\text{room}}$ ) and ordering (at “warm” deformation,  $T \leq 0.3 T_{\text{melt}}$  [1]). The deformation–induced ordering is an accelerated one and comparable with the action-influence of high-energy electrons at relatively moderate temperatures. In particular, in binary bcc Fe-Mn and Fe-Cr and fcc Fe-Ni alloys it was shown using method of Mössbauer spectroscopy that severe plastic deformation via high pressure torsion (HPT) and milling in ball mills at temperatures close to room temperature, each is accompanied with short-range ordering (SRO) comparable (in degree) with the ordering accelerated due to an irradiation by high-energy electrons of fluence  $F \sim 5 \times 10^{22} \text{ m}^{-2}$  within a nearby range of temperatures [3,6–9]. Based on the results obtained, a conclusion was drawn on that accelerated ordering is the consequence of (the presence of) moveable vacancy complexes. The SRO (order) formation as the initial stage of phase transitions affects the alloy properties and,

in particular, the stability of the structure in conditions of intense irradiation and deformation-related effects. In this regard, studies of short-range ordering in Fe-Cr alloys, as well as of the effect exerted on this ordering by introduced impurities, are important along with the fact that bcc Fe-Cr alloys are the basis of irradiation-resistant stainless steels of the ferrite–martensite class of such materials [10].

It is known that in iron and in Fe-Cr alloys, oversized impurities of substitution, such as Sb and Au, in conditions of irradiation just form vacancy complexes stable at a thermal annealing [11,12]. In the experiments with employment of positron-annihilation spectroscopy (PAS), the stability of vacancy complexes was determined based on the knowledge of the temperature of their dissociation from the curves of the parameter  $S$  versus temperature of heating. In the case of the alloys Fe-16Cr doped with Sb and Au, the onset (in case of each impurity) of dissociation of vacancy-impurity complexes formed as a result of irradiation with a fluence of  $F = 5 \times 10^{21} \text{ m}^{-2}$  were found to have shifted into the range of higher temperatures by 250 and 100 K, respectively [11]. Since the substitution impurities essentially weaken the mobility of vacancies in irradiated samples, it is of interest to investigate the effect of these impurities on the mechanism and kinetics of the deformation—induced SRO connected with the mobility of vacancy complexes [6].

Thus, the aim of the present work was investigation of the effect of Sb and Au impurities in the alloys Fe-16Cr on the processes of SRO using Mössbauer spectroscopy. The aim also consisted in verification of the mechanism of deformation-induced SRO with using a comparison between the results of Mössbauer investigation and the data of PAS on the mobility of the vacancy complexes accumulated in the course of irradiation by electrons of the binary and doped alloys with impurities of Sb and Au.

## 2. Materials and Methods of Investigation

The objects of investigation were Fe-Cr alloys with bcc crystal lattice: the binary alloy Fe-16Cr and one additionally doped with the impurities of antimony: Fe-16Cr-0.3Sb and gold: Fe-16Cr-0.13Au, see Table 1. The concentrations of Sb and Au were controlled by weighting and confirmed by the methods of Rutherford backscattering and X-ray microanalysis. For a more correct comparison of Mössbauer and PAS data, the investigations were performed on the same samples [11]. The procedure of preparation of alloys is described in [13]. After rolling, cutting, and electrical polishing, the samples about  $10 \times 10 \text{ mm}^{-2}$  in size ( $\sim 0.3 \text{ mm}$  thick) were annealed under  $10^{-5} \text{ Pa}$  vacuum at 1070 K (in ferritic area) for 4 h followed by air cooling. This state of the materials is further referred to as initial.

**Table 1.** Composition of Fe-Cr alloys

Alloy	Cr, at % ( $\pm 0.1$ )	Sb, at % ( $\pm 0.05$ )	Au, at % ( $\pm 0.02$ )	Ni, at %	N, at %
Fe-16Cr	16.0	-	-	<0.01	<0.01
Fe-16Cr-0.3Sb	16.0	0.30	-	<0.01	<0.01
Fe-16Cr-0.13Au	16.0	-	0.13	<0.01	<0.01

Severe plastic deformation was performed by HPT in Bridgman anvils to the degree  $\varepsilon = 5.9$  ( $n = 3$  revolutions of anvils) and rate  $2.4 \times 10^{-2} \text{ s}^{-1}$  (0.3 rev/min) at temperatures of from 298 to 673 K, in a way similar to that from [3,6–8]. The degree of true deformation was estimated by the formula [14].

The scheme of experiment is shown in [7]. The required temperature was achieved usually within 10 or 20 min after placing the anvils with a sample into liquid nitrogen or furnace, respectively. Then a sample at the given temperature was loaded to a pressure of 8 GPa and subjected to deformation torsion by rotating the bottom anvil. The time of HPT was 10 min. After the torsion, the sample was returned to room temperature and unloaded. After that, samples had a shape of a disc of 7 mm in diameter and 150  $\mu\text{m}$  in thickness. For Mössbauer measurements, the disc was thinned, first, mechanically with diamond paste and then electrochemically up to 20  $\mu\text{m}$ . For the Mössbauer measurements, there was used either a full surface area of the sample. Apart from the experiment on HPT, the initial samples were annealed at 773 K, for 1 h.

Mössbauer  $\gamma$ -quantum absorption spectra on  $^{57}\text{Fe}$  were obtained at room temperature in the mode of constant acceleration with the  $^{57}\text{Co}(\text{Rh})$  source. As a calibration standard, that one of an iron foil was used. The measurements were carried out on the 20  $\mu\text{m}$  thick foils.

A package of special programs [15] was used for the calculation of Mössbauer spectra. The calculation included the restoration of both distribution of the hyperfine magnetic field  $p(H)$ . Then the distribution  $p(H)$  was used for the modeling and approximation of experimental Mossbauer spectra by a sum of several sub-spectra, sextets  $A(N_1, N_2)$ , either of which corresponded to the various possible distributions of Cr atoms in the nearest coordination shells (CSs) of  $^{57}\text{Fe}$  atoms referred further to as the atomic configurations  $(N_1, N_2)$ . Here  $N_1$  and  $N_2$  are the numbers of chromium atoms in the first and second CSs, respectively. The integral intensity of each sextet  $A(N_1, N_2)$  is proportional to the probability  $W(N_1, N_2)$ , namely, the probability of finding  $N_1$  chromium atoms in the first and  $N_2$  atoms of chrome in the second CS.

The redistribution of atoms during SRO formation was analyzed by means of Mössbauer spectra in the same way as it was done in [3,6,16–19], i.e., considering various possible distributions of Cr atoms in the two nearest coordination shells (CSs) of  $^{57}\text{Fe}$  atoms. The hyperfine parameters (of spectra)  $X = H$  (magnetic field) or  $I_s$  (isomer shift) were additive, i.e.,  $X(N_1, N_2) = X(0, 0) + N_1 \cdot \Delta X_1 + N_2 \cdot \Delta X_2$ , where  $X(0, 0)$  is the value of the parameters in the absence of impurity of chromium (Cr),  $\Delta X_1$  and  $\Delta X_2$  are the changes of  $X$  due to one Cr atom in the first and the second CSs. The values of  $\Delta H_1$  and  $\Delta H_2$  were  $32(\pm 1)$  and  $20(\pm 1)$  kOe, respectively.

When simulating spectra of the alloys with the impurities of Sb and Au, the influence of the latter on the hyperfine parameters were neglected because of the small (just tenths of an atomic percent) concentration of the impurities. The same circumstance concerns the effect of vacancies. In accordance with [20,21], after HPT, their concentration does not exceed the value  $4\text{--}5 \times 10^{-4}$  of relative units. The probabilities  $W(N_1, N_2)$  of observing in the first and second CSs the different number of Cr atoms without formation of the SR or the long-range (LR) order were taken as correspondent to binomial distribution. In the case of the formation of SR order in an  $\text{Fe}_{100-c}\text{Cr}_c$  alloy, the average concentrations of the Cr component over the first and second (nearest) CSs differ from that characteristic of disordered state and are equal to  $c_1 = c \cdot (1 - \alpha_1)$  and  $c_2 = c \cdot (1 - \alpha_2)$ , respectively, where  $\alpha_i$  are the Cowley parameters of SRO in the  $i$ -th CS [4]. The effective—i.e., averaged over two CSs—chromium concentration  $c_{1,2}$  is determined by relationship [19]

$$c_{1,2} = \frac{Z_1 \cdot c_1 + Z_2 \cdot c_2}{Z_1 + Z_2}, \quad (1)$$

where  $Z_1 (= 8)$  and  $Z_2 (= 6)$  are the coordination numbers.

The total contribution of these sextets, i.e.,  $\sum A(N_1, N_2)$ , was about 95%, see Tables 2–4. Only sextets with partial contribution exceeding 1% were taken into account in spectra approximation, i.e.,  $A(N_1, N_2) \geq 1\%$ .

The validity of such modeling and estimating  $c_{1,2}$  is confirmed by comparison of the theoretically calculated  $W_{\text{theor}}$  and spectra approximation, see Figures 1–3 and Tables 2–4. In the case of statistically random distribution of atoms over the lattice sites, the value of  $c_{1,2} = c_{1,2(\text{random})}$  and  $\alpha_{1,2} = 0$ . In the case of SR ordering, i.e., tendency to neighboring between different atoms,  $c_{1,2} > c_{1,2(\text{random})}$  and  $\alpha_{1,2} < 0$ . In the other case, i.e., SR clustering with a tendency to neighboring between similar atoms,  $c_{1,2} < c_{1,2(\text{random})}$  and  $\alpha_{1,2} > 0$ .

Besides, to obtain the qualitative estimation of redistribution, the linear dependence of the average effective field  $\langle H \rangle$  (kOe) on the chromium concentration  $c$  (at %) in Fe-Cr alloys [6], namely,

$$\langle H \rangle = 330 - k \cdot c, \quad (2)$$

was used additionally, where the coefficient of proportionality  $k = 2.83 \text{ kOe} \times \text{at}^{-1}$ . This dependence was obtained based on the calculated values of the average effective field in the (initial) Fe-Cr alloys annealed at 1073 K and found to be close to that in [14–17] where  $Z_1 (= 8)$ .

Mössbauer data on the deformation-induced ordering of the alloys were compared with the PAS data on the dissociation of vacancy defects during annealing of the samples preliminarily irradiated by electrons [9].

**Table 2.** Hyperfine parameters\* and contributions of subspectra for the Fe-16Cr alloy. Subspectra contributions are presented for random distribution ( $A_{\text{theor}}$ ), initial state ( $A_i$ ) and after HPT at 298 K ( $A_{298}$ ) and 623 K ( $A_{623}$ ).

Configuration (N1,N2)	Isomer Shift Is, mm/s ( $\pm 0.010$ )	Hyperfine Magnetic Field H, kOe ( $\pm 1$ )	Sub-Spectrum Contribution			
			A <sub>theor</sub> , %	A <sub>i</sub> , % ( $\pm 1$ )	A <sub>298</sub> , % ( $\pm 1$ )	A <sub>623</sub> , % ( $\pm 1$ )
0.0	0.014	341	8.7	12	9	12
0.1	−0.006	321	9.0	7	10	13
1.0	−0.014	310	13.7	17	14	15
0.2	−0.031	300	4.7	11	5	11
1.1	−0.037	288	15.2	12	15	12
0.3	−0.041	280	1.2	2	5	2
2.0	−0.047	276	8.8	9	9	8
1.2	−0.055	268	7.2	8	9	6
2.1	−0.062	258	10.1	10	9	10
1.3	−0.074	248	1.8	1	3	1
3.0	−0.070	245	3.4	4	4	5
2.2	−0.080	236	4.8	3	4	2
3.1	−0.090	225	3.8	2	3	2
2.3	−0.100	216	1.2	2	1	1

\* G (line width) for as-received, irradiated and aged states is 0.34 mm/s, for HPT—0.35 mm/s. Values of quadrupole splitting (Qs) are close to zero and are not shown.  $S(N_1, N_2) < 1\%$  are not shown.

**Table 3.** Hyperfine parameters\* and contributions of subspectra for the Fe-16Cr-Sb alloy. Subspectra contributions are presented for random distribution ( $A_{\text{theor}}$ ), initial state ( $A_i$ ) and after HPT at 298 K ( $A_{298}$ ) and 673 K ( $A_{673}$ ).

Configuration (N1,N2)	Isomer Shift Is, mm/s ( $\pm 0.010$ )	Hyperfine Magnetic Field H, kOe ( $\pm 1$ )	Sub-Spectrum Contribution			
			A <sub>theor</sub> , %	A <sub>i</sub> , % ( $\pm 1$ )	A <sub>298</sub> , % ( $\pm 1$ )	A <sub>673</sub> , % ( $\pm 1$ )
0.0	0.012	341	8.7	12	9	11
0.1	−0.008	321	9.0	6	7	6
1.0	−0.016	310	13.7	18	12	18
0.2	−0.025	300	4.7	11	10	11
1.1	−0.033	288	15.2	12	15	13
0.3	−0.040	280	1.2	4	2	2
2.0	−0.043	276	8.8	7	9	9
1.2	−0.050	268	7.2	9	10	8
2.1	−0.058	258	10.1	10	11	8
1.3	−0.072	248	1.8	1	2	1
3.0	−0.067	245	3.4	2	1	5
2.2	−0.073	236	4.8	4	7	4
3.1	−0.083	225	3.8	2	4	1
2.3	−0.095	216	1.2	1	1	2

\* G (line width) for as-received, irradiated and aged states is 0.34 mm/s, for HPT—0.35 mm/s. Values of quadrupole splitting (Qs) are close to zero and are not shown.  $S(N_1, N_2) < 1\%$  are not shown.

**Table 4.** Hyperfine parameters\* and contributions of subspectra for the Fe-16Cr-Au alloy. Subspectra contributions are presented for random distribution ( $A_{\text{theor}}$ ), initial state ( $A_i$ ) and after HPT at 298 K ( $A_{298}$ ) and 573 K ( $A_{573}$ ).

Configuration ( $N_1, N_2$ )	Isomer Shift $I_s$ , mm/s (0.010)	Hyperfine Magnetic Field $H$ , kOe ( $\pm 1$ )	Sub-Spectrum Contribution			
			$A_{\text{theor}}$ , %	$A_i$ , % ( $\pm 1$ )	$A_{298}$ , % ( $\pm 1$ )	$A_{573}$ , % ( $\pm 1$ )
0.0	0.015	341	8.7	11	9	12
0.1	-0.005	321	9.0	10	10	11
1.0	-0.013	310	13.7	12	13	14
0.2	-0.025	300	4.7	11	11	11
1.1	-0.033	288	15.2	12	14	13
0.3	-0.045	280	1.2	2	2	2
2.0	-0.041	276	8.8	12	9	8
1.2	-0.050	268	7.2	6	8	8
2.1	-0.058	258	10.1	11	10	9
1.3	-0.073	248	1.8	1	2	1
3.0	-0.066	245	3.4	3	2	2
2.2	-0.080	236	4.8	4	5	4
3.1	-0.085	225	3.8	3	3	3
2.3	-0.096	216	1.2	1	2	2

\*  $G$  (line width) for as-received, irradiated and aged states is 0.34 mm/s, for HPT—0.35 mm/s. Values of quadrupole splitting ( $Q_s$ ) are close to zero and are not shown.  $S(N_1, N_2) < 1\%$  are not shown.

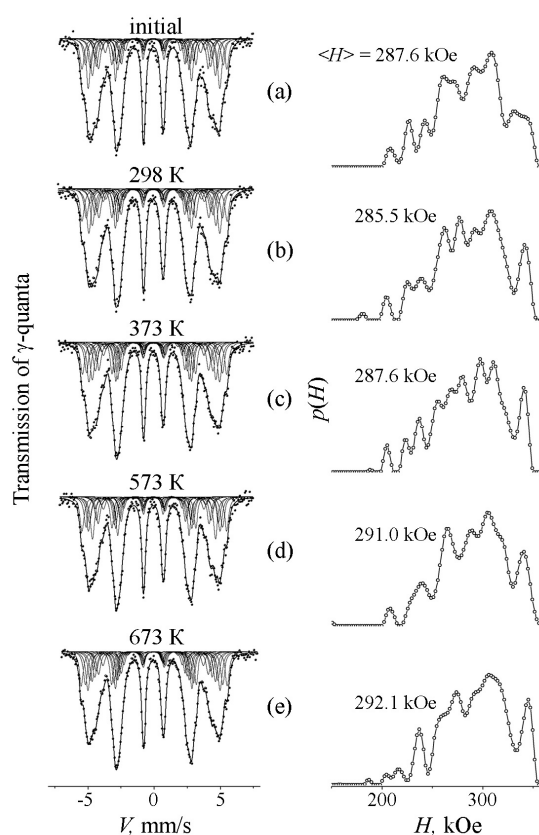


**Figure 1.** Mössbauer spectra, distributions  $p(H)$ , and values of  $\langle H \rangle$  for the alloy Fe-16Cr in the initial state and after—HPT ( $\epsilon = 5.9$ ,  $n = 3$  rev.) at different temperatures: (a)—initial state (annealed at 1073 K, 4 h); (b)—HPT at 298 K; (c)—HPT at 373 K; (d)—HPT at 573 K, and (e)—HPT at 673 K. Mössbauer spectra were measured at room temperature.

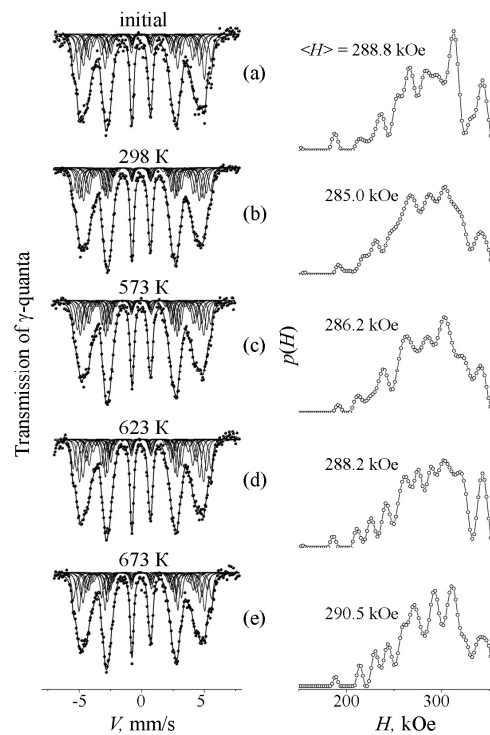


**Figure 2.** Mössbauer spectra, distributions  $p(H)$ , and values of  $\langle H \rangle$  for the alloy Fe-16Cr-Sb in the initial state and after HPT ( $\epsilon = 5.9$ ,  $n = 3$  rev.) at different temperatures: (a)—initial state (annealed at 1073 K, 4 h); (b)—HPT at 298 K; (c)—HPT at 573 K; (d)—HPT at 623 K, and (e)—HPT at 673 K. Mössbauer spectra were measured at room temperature.

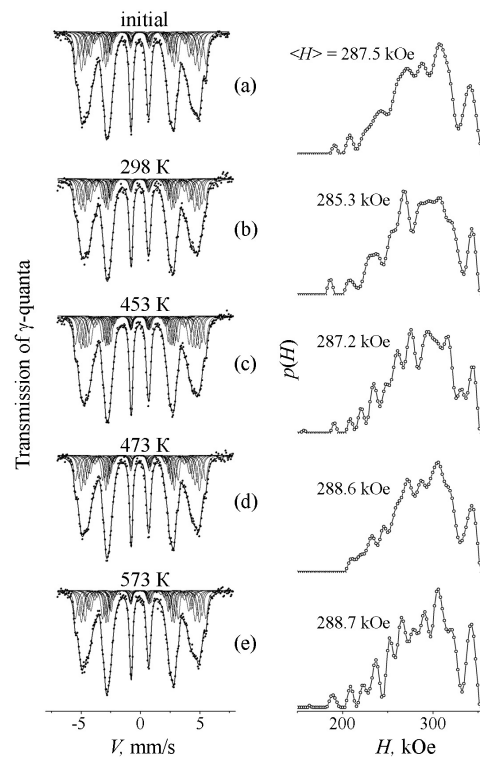


**Figure 3.** Mössbauer spectra, distributions  $p(H)$ , and values of  $\langle H \rangle$  for the alloy Fe-16Cr-Au in the initial state and after HPT ( $\epsilon = 5.9$ ,  $n = 3$  rev.) at different temperatures: (a)—initial state (annealed at 1073 K, 4 h); (b)—HPT at 298 K; (c)—HPT at 453 K; (d)—HPT at 473 K, and (e)—HPT at 573 K. Mössbauer spectra were measured at room temperature.

### 3. Experimental Results

In Figures 1–3 we present the spectra, distributions  $p(H)$ , and values  $\langle H \rangle$  for the alloy samples—initial and HPT—deformed at different temperatures. It is seen that the smallest of the values of  $\langle H \rangle$  was obtained after HPT at 298 K and, further,  $\langle H \rangle$  grows steadily when increasing HPT temperature to 673 K, see Figure 4. The growth of  $\langle H \rangle$  was stipulated by increasing contribution to  $p(H)$  from Cr-depleted atomic surroundings of iron. These contributions of  $W(N_1, N_2) = \sum A(N_1, N_2)$  are the probabilities of an occupation of the first two CSs of iron by Cr atoms of number  $N_{1,2} = N_1 + N_2 = 0, 1$ . The fields of these surroundings are of larger magnitude, see Tables 2–4. Note that, with lowering chromium concentration, an effective field at an iron atom tends to increase; thus, the growth of  $\langle H \rangle$  proceeds at the expense of lowering the number of atomic configurations with  $N_{1,2} = N_1 + N_2 \geq 2$ .

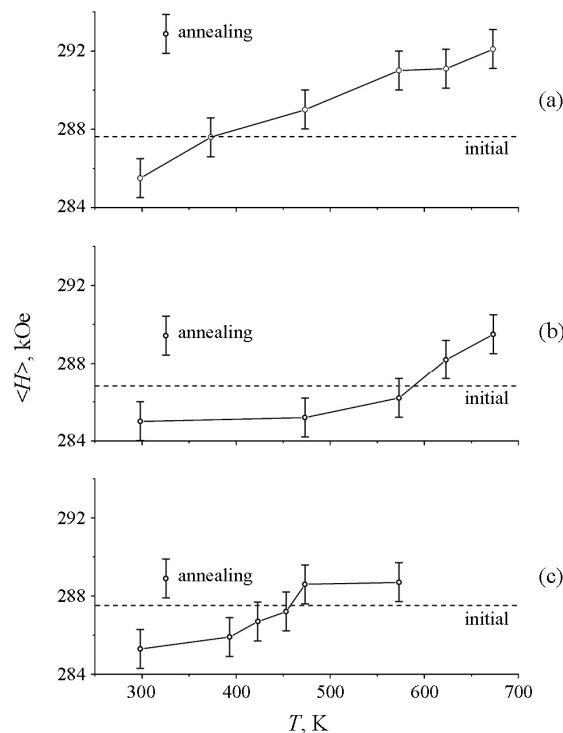


**Figure 4.** Dependence of  $\langle H \rangle$  on the temperature of deformation of alloys: (a)—Fe-16Cr, (b)—Fe-16Cr-Sb, and (c)—Fe-16Cr-Au. Dash line designates the value of field  $\langle H \rangle$  in the initial state of the alloys. Dot designates the value of  $\langle H \rangle$  in the alloys after annealing at 773 K, 1 h.

In accordance with the Equations (1) and (2), the growth of  $\langle H \rangle$  testifies to the decrease in  $c_{1,2}$  at raising the temperature of deformation of samples from 298 K. However, in relation towards “initial” samples, the changes in the occupations  $W(N_1, N_2) \sim A(N_1, N_2)$ ,  $\langle H \rangle$ , and  $c_{1,2}$  with changing HPT temperature are not regular. The behavior of parameters of the deformed samples in relation to the parameters of the initial state of alloys can be conventionally classified into two regions of temperatures. The first region (of cold deformation) represents the temperatures of HPT, at which one can observe the decrease in the contribution from Cr-depleted (i.e., with  $N_1 = 0, 1$ ) atomic configurations, the decrease in  $\langle H \rangle$ , and the growth in the effective concentration  $c_{1,2}$ —in relation to corresponding initial samples. For the alloy Fe-16Cr, as well as for the alloys Fe-13.2Cr and Fe-20.6Cr [6], “cold” deformation (298 K) leads to a decrease in  $\langle H \rangle$  and to a growth of  $c_1$ , as a consequence of destruction of regions of the short-range order of separation origin that were present in the initial state, see Figures 4a and 5a, and Table 2. The second region of temperatures (of “warm” deformation) is characterized by opposite changes, namely, by growth of the contribution from depleted configurations, by growth of  $\langle H \rangle$ , and by a decrease in  $c_{1,2}$  of deformed samples in relation to an initial sample, i.e., by the process of SR

ordering of separation origin. For the alloy Fe-16Cr, the region of “warm” deformation, connected with the decrease in  $c_{1,2}$ , commences at temperatures above 373 K, Figures 4a and 5a.

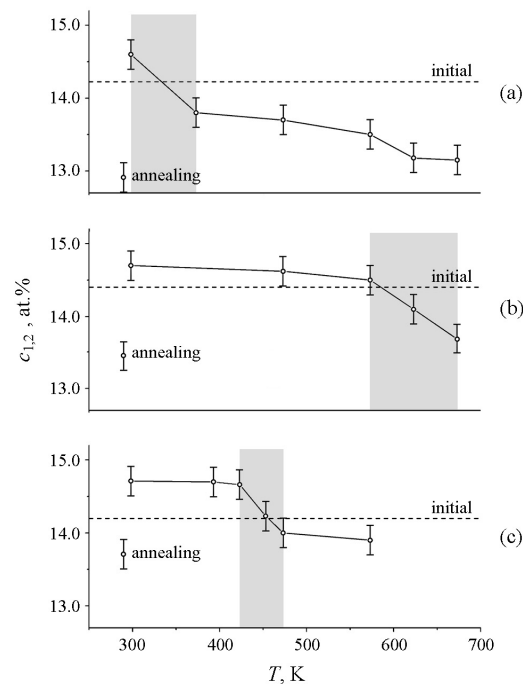


**Figure 5.** Dependence of  $c_{1,2}$  on the temperature of deformation of alloys: (a)—Fe-16Cr; (b)—Fe-16Cr-Sb, and (c)—Fe-16Cr-Au. Dash line designates the value of  $c_{1,2}$  in the initial state of the alloys. Dot designates the value of  $c_{1,2}$  in the alloys after annealing at 773 K, 1 h. Darkening marks the region of accelerated altering of  $c_{1,2}$  vs. the temperature of deformation.

In the alloy doped with Sb, the HPT temperature region (outside it one can observe SR ordering as a result of concentration separation) is situated above 250 K relative to that of the binary alloy Fe-16Cr, Figures 4b and 5b and Table 3. The HPT of the alloy Fe-16Cr-0.3Sb at 623 K virtually does not change the values  $\langle H \rangle$  and  $c_{1,2}$  of the «initial» sample. The decrease in  $c_{1,2}$  from 14.4 at % (for the initial sample) to 13.7 at % takes place only after HPT at 673 K, closely approaching the value of  $c_{1,2} = 13.4$  at % obtained in result of annealing at 773 K, for 1 h.

The results of HPT experiments on the alloy Fe-16Cr-0.13Au concerning the dependence of  $\langle H \rangle$  and  $c_{1,2}$  on the temperature of deformation are presented in Figures 4c and 5c. The same as in the case of the alloy with Sb, there is observed a shift of the temperature border of changing the behavior of  $\langle H \rangle$  and  $c_{1,2}$ , which characterize the degree of SRO in the samples towards higher temperatures—approximately by 100 K.

The region of the temperature border of the deformation after which one can observe realization of SR ordering in the alloys studied, is characterized by an enhanced rate of alteration of  $c_{1,2}$ , see Figure 4a–c. For the alloy Fe-16Cr this region is situated in the vicinity of 330 K, for the alloy Fe-16Cr-0.3Sb this region is situated in the vicinity of 620 K, and for the alloy F-16Cr-0.13Au in the vicinity of 450 K. Above the border mentioned the derivative from  $c_{1,2}$  by the temperature of deformation is lowered.

#### 4. Discussion

The fact of existence of a temperature border—a change in the behavior of the parameters of spectra and in  $c_{1,2}$ , which characterize the process of SR ordering, is a consequence of the concurrence between two processes, namely, disordering action of moving dislocations and ordering in result of generating a large quantity of mobile point defects [2–4,8,20–22]. The first process (dislocation disordering) little

depends on the temperature of deformation [3,6]. As is seen from Figure 5 and Tables 2–4, “cold” deformation of the binary alloy Fe–16Cr and alloys doped with Sb and Au brings the values of  $W(N_{1,2}) \sim A(N_{1,2})$  and  $c_{1,2}$  to their theoretical values  $W_{\text{theor}}$  and  $c_{1,2(\text{random})}$  which correspond to a random distribution of chromium in the solid solution. Such an action of HPT testifies to the “disintegration” of the SR order that existed in the initial state of the alloy. The “disintegration” of the SR order was observed on the samples of Fe<sub>100-c</sub>Cr<sub>c</sub> ( $c = 12 \dots 20.6$ ) alloys preliminarily aged at 773 K, for 50 h [6], as well as on the other alloys [3,7,8]. The second process (i.e., ordering that is stipulated by generation of mobile point defects) is strongly dependent on the temperature, and manifests itself already at the temperatures close to room temperature. This is seen in the steady growth of  $\langle H \rangle$  and decreasing of  $c_{1,2}$  at raising the temperature of deformation from 298 K to 673 K. The process of SR ordering at “warm” deformation is an accelerated one and takes place during the time period of 10 min (3 revs of anvils at a speed of 3 rev/min.) and it—by the degree of SRO—is close to that one accelerated (i) by the irradiation with high-energy electrons in the region of close temperatures of 400–600 K [3,6] or (ii) at thermal annealing performed at 773 K, 1 h, see Figures 4 and 5. The temperature border of the start of the process of SR ordering corresponds to the dominance of the mechanism of the ordering accelerated in relation to the concurrent process of dislocation disordering.

The doping with the impurities Sb and Au, preserving a qualitatively general form of the dependence of  $c_{1,2}$  on the HPT temperature, shifts the border between the first and the second regions of temperatures by ~250 K and by ~100 K in the alloys with Sb and with Au, respectively, in relation towards that typical of the binary alloy Fe–16Cr. To elucidate the mechanism of the effect of a substitution impurity on the deformation-induced process of SR ordering, in the present investigation we have made a comparison between our results and PAS data [11] on the evolution of vacancy defects in alloys of similar compositions, see Figure 6. Positrons are a sensitive indication of the start of stabilization of defects of vacancy type [23]. If a positron is trapped on the vacancy-type defects (small 3–D vacancy clusters), the value of  $S$  parameter increases [11–13]. The dependence of  $S$  parameter of the binary and doped alloys irradiated by electrons has a form of the curve with saturation as a result of stabilization of vacancy complexes in the course of increasing the fluence. This shows that the clusters and complexes are dominant sinks for vacancies that are mobile in conditions of irradiation at  $T_{\text{room}}$  [24,25]. In Figure 6 [11], there are presented PAS data on the dependence of  $S$  parameter when annealing vacancy defects obtained via electrons irradiation of the Fe–Cr binary and doped alloys with Sb and Au. After irradiation with a fluence of  $5 \times 10^{21} \text{ m}^{-2}$ , in Fe–Cr alloys doped with Sb and Au, the decrease of  $S$  parameter commences in the region of annealing temperatures higher by 250 and 100 K than those characteristic of the alloy Fe–16Cr, see Figure 6 [11]. This means that in the alloys doped with Sb and Au the greater part of mobile vacancies that are formed in the course of irradiation just get stabilized, in other words, form immobile vacancy complexes with Sb and Au atoms. The anneals at higher temperatures, namely, of 400, 600, and 700 K, of the alloys Fe–16Cr, Fe–16Cr–0.13Au, and Fe–16Cr–0.3Sb, respectively, lead to the decline of  $S$  parameter as a consequence of dissociation of vacancy complexes. Earlier [3,6], on the binary Fe–Cr alloys, the deformation-induced acceleration of short-range (SR) ordering in conditions of raising the HPT temperature was explained as the result of saturation of the structure by the vacancy complexes [20,21], the mobility of which strongly depends on the temperature. As it follows from the comparison between Mössbauer and PAS data, the temperature boundary (TB) between “cold” and “warm” deformation in the vicinity of which the increase in the derivative of  $c_{1,2}$  is observed, this TB coincides with the beginning of an active decrease in the parameter  $S$  at annealing of preliminarily irradiated samples. This means that the processes of SR ordering of concentration–separation origin in the HPT experiments coincide with the start of movement of vacancies as a consequence of dissociation of vacancy complexes. The impurities Sb and Au just form with the vacancies right immobile complexes and, thus, stabilize vacancies up to 600 K. At temperatures above 600 K, vacancy complexes dissociate, vacancies acquire mobility and participate in the processes of SR ordering.

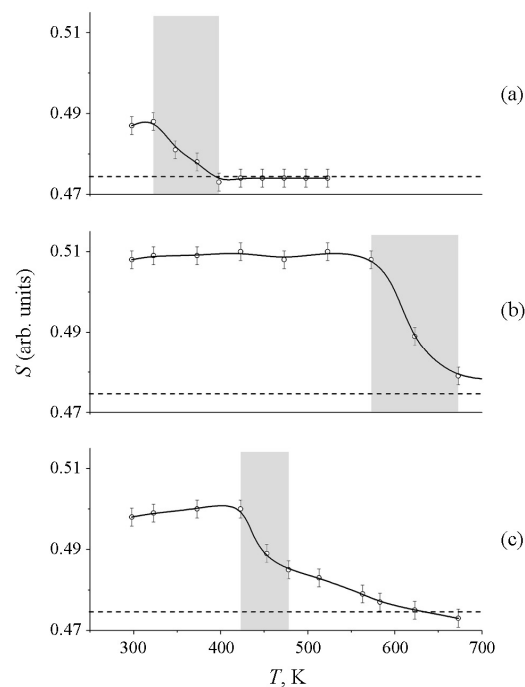


**Figure 6.** Recovery of the value of the  $S$  parameter (data from [11]) in the alloys (a)—Fe-16Cr; (b)—Fe-16Cr-Sb, and (c)—Fe-16Cr-Au irradiated at room temperature by electrons with fluence of  $5 \times 10^{21} \text{ m}^{-2}$ . The dashed line indicates the level of the  $S$  parameter value characteristic of positron annihilation in the case of bulk Fe. Darkening marks the region of the accelerated reduction of the  $S$  parameter (added by the authors).

Thus, the correlation between the temperature boundary (which characterizes an acceleration of SR ordering) and the data [11] on the temperature of the beginning of the dissociation of “vacancy-impurity” complexes, confirms the participation of vacancy complexes in the SRO processes upon deformation. We can conclude that a shift of the beginning of SRO in the direction of increasing temperature in the alloys doped with Sb and Au is due to the (i) strengthening of the bonds between vacancies and impurities and, thus, (ii) increasing of the mobility of the vacancies.

The data obtained in this work, on the temperature boundary of deformation-induced SR ordering, can employ Mössbauer spectroscopy to further investigate (i) the mobility of vacancy complexes and (ii) the bond energy between vacancies and impurities in Fe-Cr alloys.

## 5. Conclusions

Via methods of Mössbauer spectroscopy, there has been studied the mechanism of the short-range ordering induced by severe plastic deformation of/in the ferritic binary alloy Fe-16Cr, as well as in the alloys Fe-16Cr-0.3Sb and Fe-16Cr-0.13Au doped with Sb and Au. The conditional presence is established of two temperature regions of changing of the degree of short-range ordering in the course of HPT action, namely, the region of (the) “cold” deformation after which the degree of SR order (SRO) in the initial state of the alloy exhibits a decrease, and the range of (the) “warm” deformation that entails an increase in the degree of the SRO. It is shown that the temperature boundary between regions of the “cold” and the “warm” deformation is dependent on the degree of alloy’s doping with the oversized impurities Sb and Au and experiences a shift (of increase) by  $\sim 250$  (Sb) and  $\sim 100$  (Au) K in comparison with the case of the binary alloy Fe-16Cr. A comparison between the results of Mössbauer spectroscopy on the degree of (the) SRO and data of positron annihilation on the temperature of dissociation of defects of “vacancy-impurity” type has confirmed the relation between the mechanism of deformation-induced short-range ordering in Fe-Cr alloys and vacancy complexes that form in the course of severe plastic deformation.

**Author Contributions:** Conceptualization, V.S.; methodology, V.S., T.T., E.N., and A.Z.; validation, V.S. and K.K.; formal Analysis, V.S., A.Z., and K.K.; investigation, V.S. and K.K.; writing—original draft preparation, V.S. and K.K.; writing—review and editing, V.S., K.K., and Y.U.; Project Administration, V.S.; funding acquisition, V.S. All authors have read and agreed to the published version of the manuscript.

**Funding:** The research was carried out within the state assignment of Ministry of Science and Higher Education of the Russian Federation (theme “structure” no. AAAA-A18-118020190116-6) supported in part by the Russian Foundation for Basic Research grant (project no. 18-03-00216).

**Acknowledgments:** The authors express their thanks to Alexander Nikolaev for provided samples, data, and helpful discussions.

**Conflicts of Interest:** The authors declare no conflict of interest.

## References

1. Glezer, A.M.; Metlov, L.S. Physics of megaplastic (severe) deformation in solids. *Phys. Sol. State* **2010**, *52*, 1162–1169. [[CrossRef](#)]
2. Sagaradze, V.V.; Shabashov, V.A. Anomalous diffusion phase transformations in steels upon intensive cold deformation. *Phys. Met. Metall.* **2011**, *112*, 146–164. [[CrossRef](#)]
3. Shabashov, V.; Sagaradze, V.; Kozlov, K.; Ustyugov, Y. Atomic order and submicrostructure in iron alloys at megaplastic deformation. *Metals* **2018**, *8*, 995. [[CrossRef](#)]
4. Razumov, I.K.; Gornostyrev, Y.N.; Ermakov, A.E. Scenarios of nonequilibrium phase transformations in alloys depending on the temperature and intensity of plastic deformation. *Phys. Met. Metall.* **2018**, *112*, 1133–1140. [[CrossRef](#)]
5. Sakai, T.; Belyakov, A.; Kaibyshev, R.; Miura, H.; Jonas, J.J. Dynamic and post-dynamic recrystallization under hot, cold and severe plastic deformation conditions. *Prog. Mater. Sci.* **2014**, *60*, 130–207. [[CrossRef](#)]
6. Shabashov, V.A.; Kozlov, K.A.; Nikolaev, A.L.; Zamatovskii, A.E.; Sagaradze, V.V.; Novikov, E.G.; Lyashkov, K.A. The short-range clustering in Fe–Cr alloys enhanced by severe plastic deformation and electron irradiation. *Philos. Mag.* **2020**, *100*, 1–17. [[CrossRef](#)]
7. Shabashov, V.A.; Kozlov, K.A.; Sagaradze, V.V.; Nikolaev, A.L.; Semyonkin, V.A.; Voronin, V.I. Short-range order clustering in BCC Fe–Mn alloys induced by severe plastic deformation. *Philos. Mag.* **2018**, *98*, 560–576. [[CrossRef](#)]
8. Shabashov, V.A.; Kozlov, K.A.; Zamatovskii, A.E.; Lyashkov, K.A.; Sagaradze, V.V.; Danilov, S.E. Short-range atomic ordering accelerated by severe plastic deformation in FCC invar Fe–Ni alloy. *Phys. Met. Metall.* **2019**, *120*, 686–693. [[CrossRef](#)]
9. Kozlov, K.; Shabashov, V.; Zamatovskii, A.; Novikov, E.; Ustyugov, Y. Inversion of the sign of the short-range order as a function of the composition of Fe–Cr alloys at warm severe plastic deformation and electron irradiation. *Metals* **2020**, *10*, 659. [[CrossRef](#)]
10. Panin, V.E.; Derevyagina, L.S.; Lemeshev, N.M.; Korznikov, A.V.; Panin, A.V.; Kazachenok, M.S. On the nature of low-temperature brittleness of BCC steels. *Phys. Mesomech.* **2014**, *17*, 89–96. [[CrossRef](#)]
11. Druzhkov, A.P.; Nikolaev, A.L. Effects of solute atoms on evolution of vacancy defects in electron-irradiated Fe–Cr-based alloys. *J. Nucl. Mat.* **2011**, *408*, 194–200. [[CrossRef](#)]
12. Moser, P.; Corbel, C.; Lucasson, P.; Hautajarvi, P. Impurity effects on the vacancy clustering process in electron irradiated iron dilute alloys studied by positron techniques. *Mater. Sci. Forum* **1987**, *15–18*, 925–930. [[CrossRef](#)]
13. Nikolaev, A.L. Stage I of recovery in 5 MeV electron-irradiated iron and iron–chromium alloys: The effect of small cascades, migration of di-interstitials and mixed dumbbells. *J. Phys. Condens. Matter* **1999**, *11*, 8633–8644. [[CrossRef](#)]
14. Degtyarev, M.V.; Chashchukhina, T.I.; Voronova, L.M.; Patselov, A.M.; Pilyugin, V.P. Influence of the relaxation processes on the structure formation in pure metals and alloys under high-pressure torsion. *Acta Mater.* **2007**, *55*, 6039–6050. [[CrossRef](#)]
15. Rusakov, V.S.; Kadyrzhanov, K.K. Mössbauer spectroscopy of locally inhomogeneous systems. *Hyperfine Interact.* **2005**, *64*, 87–97.
16. Dubiel, S.M.; Zukrowski, J. Mössbauer effect study of charge and spin transfer in Fe–Cr. *J. Mag. Mag. Mater.* **1981**, *23*, 214–228. [[CrossRef](#)]

17. Filippova, N.P.; Shabashov, V.A.; Nikolaev, A.L. Mössbauer study of irradiation–accelerated short-range ordering in binary Fe–Cr alloys. *Phys. Met. Metall.* **2000**, *90*, 145–152.
18. Yamamoto, H. A study on the nature of aging of Fe–Cr alloys by means of the Mössbauer effect. *Jpn. J. Appl. Phys.* **1964**, *3*, 745–748. [[CrossRef](#)]
19. Dubiel, S.M.; Zukrowski, J. Distribution of Cr atoms in a strained and strain–relaxed Fe<sub>89.15</sub>Cr<sub>10.75</sub> alloy: A Mössbauer effect study. *Phil. Mag.* **2017**, *97*, 386–392. [[CrossRef](#)]
20. Gubicza, J.; Dobatkin, S.V.; Khosravi, E. Reduction of vacancy concentration during storage of severely deformed Cu. *Mater. Sci. Eng. A* **2010**, *527*, 6102–6104. [[CrossRef](#)]
21. Cizek, J.; Janecek, M.; Srba, O.; Kuzel, R.; Barnovska, Z.; Prochazka, I.; Dobatkin, S. Evolution of defects in copper deformed by high–pressure torsion. *Acta Mat.* **2011**, *59*, 2322–2329. [[CrossRef](#)]
22. Le Caer, G.; Begin–Colin, S.; Delacroix, P. Mechano–synthesis of nanostructured materials. In *Material Research in Atomic Scale by Mössbauer Spectroscopy*; Mashlan, M., Miglierini, M., Schaaf, P., Eds.; Springer: Dordrecht, The Netherlands, 2003; pp. 11–20.
23. Eldrup, M.; Singh, B.N. Studies of defects and defect agglomerates by positron annihilation spectroscopy. *J. Nucl. Mater.* **1997**, *251*, 132–138. [[CrossRef](#)]
24. Nikolaev, A.L. Specificity of stage III in electron–irradiated Fe–Cr alloys. *Philos. Mag.* **2007**, *87*, 4847–4874. [[CrossRef](#)]
25. Dimitrov, C.; Benkaddour, A.; Corbel, C.; Moser, P. Properties of point defects in model ferritic steels. *Ann. Chim. Fr.* **1991**, *16*, 319–324.



© 2020 by the authors. Licensee MDPI, Basel, Switzerland. This article is an open access article distributed under the terms and conditions of the Creative Commons Attribution (CC BY) license (<http://creativecommons.org/licenses/by/4.0/>).